Received: 23 April 2021 | Revised: 21 September 2021 | Accepted: 21 October 2021

DOI: 10.1002/joc.7423

RESEARCH ARTICLE

International Journal of Climatology RMetS

The seasonal predictability of the wet season over Peninsular Florida

Carly D. Narotsky[1,2] | **Vasubandhu Misra**[1,2,3]

[1]Department of Earth, Ocean, and Atmospheric Science, Florida State University, Tallahassee, Florida, USA

[2]Center for Ocean-Atmospheric Prediction Studies, Florida State University, Tallahassee, Florida, USA

[3]Florida Climate Institute, Florida State University, Tallahassee, Florida, USA

Correspondence
Carly D. Narotsky, Department of Earth, Ocean, and Atmospheric Science, Florida State University, Tallahassee, FL, USA.
Email: cnarotsky@fsu.edu

Funding information
National Aeronautics and Space Administration, Grant/Award Number: NNX17AG72G

Abstract

In this study, we examine the seasonal predictability of Peninsular Florida (PF)'s boreal summer season, which is also known as the PF wet season (PFWS) due to the coinciding peak of the robust seasonal cycle of rainfall. The seasonal predictability is examined in the Community Climate System Model, version 4 (CCSM4), which is one of the models of the North American Multi-Model Ensemble used for routine, operational seasonal forecasts by the National Oceanic and Atmospheric Administration (NOAA) Climate Prediction Center (CPC). An objective definition of the onset and the demise of the PFWS are then implemented, and the predictability of the onset, the demise and the seasonal rainfall anomaly is assessed from the CCSM4 seasonal hindcasts. Our study shows that the 33 years (1983–2015) of the CCSM4 seasonal hindcasts display very poor deterministic and probabilistic skill in predicting the onset and the demise of the PFWS and its seasonal rainfall anomalies for all lead times. It is shown that the seasonal hindcasts display poor skill for both the fixed calendar month and varying seasonal length of the PFWS. In many of these instances, the skills deteriorate with the lead time of the CCSM4 hindcasts, although, in some cases, they bear no relation (e.g., demise date of the PFWS). Our analysis reveals that the interannual variability of the location of the western ridge of the North Atlantic subtropical high is poorly rendered in the seasonal hindcast of CCSM4 with respect to reanalysis. This could explain the origins of some of the potential issues of the CCSM4 seasonal hindcasts with the variability of the PFWS.

KEYWORDS

Peninsular Florida, rainfall, seasonal predictability, wet season

1 | INTRODUCTION

Peninsular Florida (PF) experiences a distinct wet season during boreal summer. In May or June, there is an abrupt onset of higher daily rain rates, which are sustained through the summer and have an abrupt demise in September or October (Misra *et al.*, 2018). The PF wet season (PFWS) replenishes the Floridan aquifer, a source of drinking water for the growing population of Florida and its neighbouring states (Lindsey *et al.*, 2009). The PFWS also sustains the unique ecosystem of the Everglades and the storm protection, tourism, and fish that come with it (NWF, 2019). In addition, the PFWS is vital for Florida's agriculture industry, which leads the nation in the production of seven crops, supports two million jobs and contributes over $120 billion in economic

impact to the state annually (Putnam, 2016). Predicting the onset and the demise of the PFWS is of practical use to farmers for choosing planting dates to optimize crop yields. Prediction of the onset of the PFWS is also valuable to land managers and policy makers who control wildfires, as the largest fires occur within a week of the onset of the PFWS (Slocum *et al*., 2007).

Misra *et al*. (2018) indicate that the observed climatological onset and demise dates of the PFWS are May 21st and October 10th, respectively. These dates have large interannual variability; the standard deviations for the onset and demise dates are 15 and 16 days, respectively, resulting in large seasonal rainfall anomalies with varying seasonal lengths (Misra *et al*., 2018). Therefore, predicting the onset and demise dates of the PFWS is useful for anticipating seasonal rainfall anomalies.

The seasonal evolution of the PFWS coincides with the seasonal evolution of sea surface temperature (SST), upper ocean heat content and currents in the Gulf of Mexico and western Atlantic Ocean, and with the seasonal evolution of upper air wind and humidity fields in the region (Misra *et al*., 2018). For example, the onset of the PFWS accompanies the seasonal warming of the surrounding oceans with the strengthening of the loop current, and the demise occurs with a weakening of the loop current and a reduction in upper ocean heat content (Misra and Mishra, 2016; Misra *et al*., 2018). Similarly, before the onset date of the PFWS, the 850 hPa winds over PF are mostly northerlies and northwesterlies. But during the PFWS, the southerlies and southwesterlies that comprise the western edge of the North Atlantic subtropical high (NASH) prevail over PF (Misra *et al*., 2018). The prediction skill of precipitation in the PFWS is poor in comparison with the winter season, which has a robust teleconnection with ENSO (Stefanova *et al*., 2012). Prior to 1976, ENSO variability influenced the PFWS too (Misra and DiNapoli, 2013). Warm or cold ENSO events in boreal winter preceded long or short wet seasons with an early or late onset, respectively. Post-1976, however, the influence of ENSO on the PFWS has diminished (Misra and DiNapoli, 2013). This may be explained by a decadal change in the dynamics of the development of El Niño events (B. Wang, 1995; B. Wang and An, 2002; C. Wang and Picaut, 2004). The warm SST anomalies associated with El Niño events in the pre-1976 period first occurred in the eastern tropical Pacific during boreal spring of the El Niño year and then spread westward. Post-1976, however, El Niño events began with warm SST anomalies in the western and central Pacific, and the warming in the eastern Pacific occurred in the boreal spring following the El Niño year. After 1976, interannual variations in the PFWS have been found to be driven by variability of the NASH (Li *et al*., 2011) and the size of the Atlantic warm pool (Misra and DiNapoli, 2013). In addition, summer rainfall variability in the contiguous United States has been found to be affected by East Asian subtropical monsoon rainfall variability via the Asia–North America (ANA) teleconnection (Zhu and Li, 2016). Furthermore, the influence of the ANA teleconnection has become enhanced since the early 1990s when the East Asian summer monsoon shifted northward, enabling the East Asian subtropical monsoon heating to induce the upper-level ANA teleconnection pattern more effectively (Zhu and Li, 2018).

In this study, we specifically examine the predictability of the onset, demise and seasonal rainfall anomalies of the PFWS from the Community Climate System Model, version 4 (CCSM4; Gent *et al*., 2011). Although the onset and the demise dates of the PFWS allude to specific days of the year, we contend that it is a seasonal predictability problem, as the onset and the demise of the PFWS are part of the seasonal cycle that evolves with the large-scale seasonal evolution of the surrounding upper oceans and upper air kinematic and thermodynamic fields (Misra *et al*., 2018). Furthermore, the onset and the demise of the PFWS appear as unique points in the time series, unlike weather events, which can occur multiple times in a season or across seasons. In addition, we are examining the variations of the wet season across PF as an aggregated (or area-averaged) value, partially because a majority of the current seasonal prediction climate models lack sufficient resolution to resolve the coastlines of Florida (e.g., Figure 1a; Misra *et al*., 2019). This aggregation or area average over PF further reduces the high-frequency variability associated with say, grid point values of a variable of the model.

2 | METHODOLOGY AND DATA

The objective technique for diagnosis of the onset/demise dates of the PFWS was first introduced in Camberlin and Diop (2003) and adapted in several other studies (e.g., Liebmann *et al*., 2007; Misra & DiNapoli, 2013; Bombardi *et al*., 2019). The onset and the demise dates of the PFWS are essentially defined to be the first and the last day of the year when the daily rain rate exceeds and recedes from the climatological annual mean rain rate, respectively (Misra *et al*., 2018). The onset and the demise dates of the PFWS are isolated by picking the minima and the maxima, respectively, in the daily cumulative anomaly curve of the area-averaged rainfall over PF ($r'_n(k)$). $r'_n(k)$ is given by:

$$r'_n(k) = \sum_{m=1}^{k} \left[r_n(m) - \bar{\bar{r}} \right], \tag{1}$$

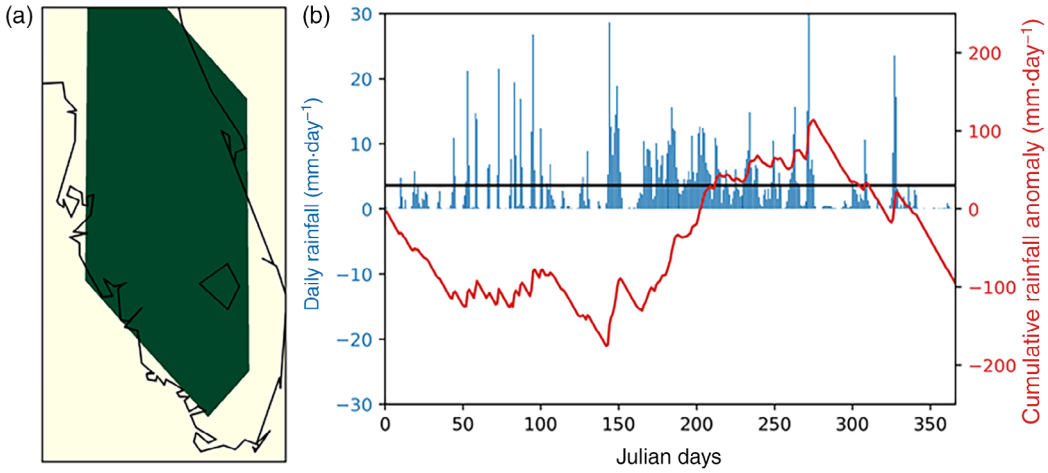

FIGURE 1 (a) The mask for PF used to compute the area average from CCSM4. (b) The illustration of the diagnosis of the onset and the demise date of the wet season over PF from observations for 1984, showing the daily area-averaged rainfall over PF (blue bars), the annual mean climatology (black line) and the corresponding cumulative rainfall anomalies (red line)

where $r_n(m)$ is the area-average daily rainfall for day m of year n averaged over PF, $\bar{\bar{r}}$ is the corresponding annual mean climatology of the rainfall, and k is the day of the year up to which the accumulation of the daily rainfall anomaly is computed. An illustration of this diagnosis for the year 1984 from observed rainfall analysis is shown in Figure 1b, with the onset and the demise dates to be May 23rd and October 3rd, respectively.

In the observations, the diagnosis of the onset/demise date is relatively trivial, as there is one onset/demise for each year. However, the diagnosis of the onset/demise date of the PFWS becomes non-trivial in the case of seasonal hindcasts that start at various times of the year and have several ensemble members per season. In this study, the CCSM4 seasonal hindcasts, which are part of the North American multi-model ensemble (NMME; Kirtman *et al.*, 2014), are initiated at the first of each month for a 12-month integration from 1983 to present (but we use only up to 2015). Constructions of the annual time series are created separately for each of the 12 hindcast lead times—from lead-0 month to lead-11 month. In addition, each seasonal hindcast consists of 10 ensemble members. Therefore, $\bar{\bar{r}}$ of Equation (1) is computed from CCSM4 seasonal hindcasts as follows:

$$\bar{\bar{r}}_i = \frac{1}{KNJ} \sum_{j=1}^{J} \sum_{n=1}^{N} \sum_{m=1}^{K} r_j(m,n), \qquad (2)$$

where i is the lead time of the hindcast going from 0 to 11 months, J is the total number of ensemble members per season, N is the number of years, and K is the number of days in the year (=365 or 366). For each year, we compute 120 model hindcasted onsets/demises from 10 ensemble members and 12 hindcast lead times of CCSM4.

The CCSM4 seasonal hindcasts are initialized using the operational climate forecast system reanalysis ocean, land and atmospheric states (Kirtman *et al.*, 2014). The daily model output is re-gridded from its native grid on a spatial resolution of 1.0° latitude × 1.0° longitude from 1983 to 2015. For precipitation verification of these hindcasts, we use the Climate Prediction Center (CPC) unified gauge-based analysis of global daily precipitation (Xie *et al.*, 2007; Chen *et al.*, 2008). The dataset is available with a spatial resolution of 0.5° latitude × 0.5° longitude over global land and with daily fields from 1979 to present.

3 | RESULTS

3.1 | Systematic errors

The observed climatological onset and demise date of the PFWS is June 1st and October 6th during 1983–2015, respectively (Figure 2a). The climatological onset dates hindcasted by CCSM4 have a late bias, which increases with lead time of the hindcast (Figure 2a). Initially at lead-0 month, the climatological onset date from the CCSM4 hindcast is June 4th, just 3 days later than the observed climatological onset date. But by lead-11 month, the hindcasted climatological onset date of the PFWS is July 20th, an error of 49 days (Figure 2a). Similarly, the 1983–2015 climatological demise dates hindcasted by CCSM4 also have a late bias (Figure 2a). At lead-0 month,

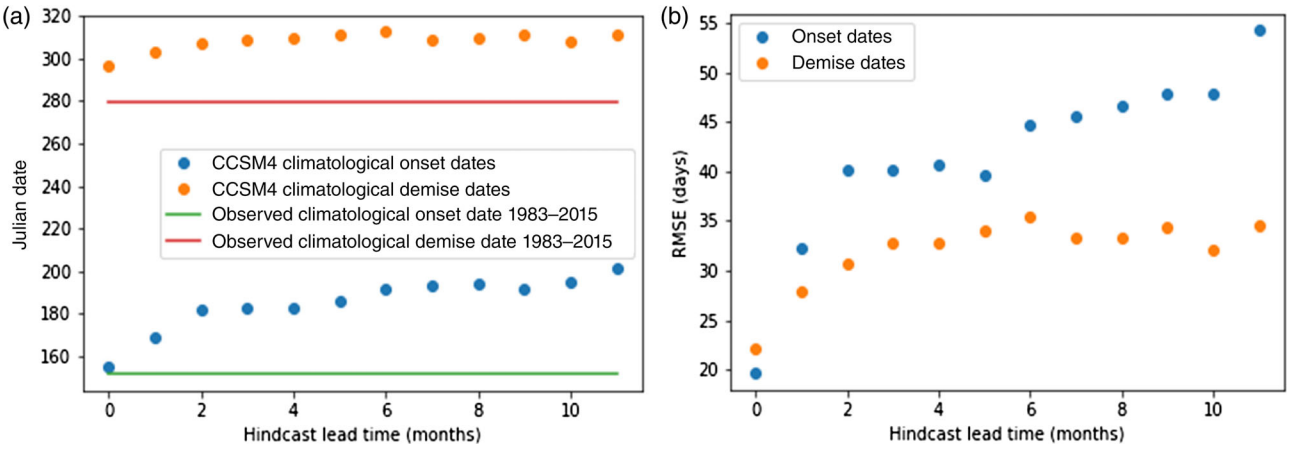

FIGURE 2 (a) The observed climatological (1983–2015) onset date (June 1st; green line) and demise date (October 6th; red line) of the PF wet season. The corresponding CCSM4 hindcast climatological onset (blue dots) and demise (orange dots) dates of the PF wet season at hindcast lead times of 0–11 months. (b) The root mean square error of the 1983–2015 onset (blue dots) and demise dates (orange dots) of the PF wet season from CCSM4 hindcast at lead times of 0–11 months

the climatological demise date hindcasted by CCSM4 is October 23rd, more than 2 weeks later than the observed climatological demise date of October 6th. The late bias increases with increasing lead time, with a late bias of 24 days at lead-1 month, and a late bias of 28 days at lead-2 month. At lead times of 3 months or more, the hindcasted demise dates remain consistently between November 4 and 8, an error of approximately 1 month (Figure 2a).

The challenge of forecasting summer-time seasonal convective precipitation over PF is well known (Stefanova *et al.*, 2012; Kirtman *et al.*, 2017). This is very well illustrated in Figure 3, which shows the root mean square error (RMSE) of monthly mean precipitation at lead-0 to lead-11 months for every month of the year from the CCSM4 hindcasts. The highest RMSEs are in the months of the wet season, particularly in June, July and August. In those months, the RMSE increases with increasing lead time. In most other months, there is no relationship between hindcast lead time and the RMSE of monthly mean precipitation (Figure 3).

3.2 | Interannual variations

3.2.1 | Deterministic skill

As indicated earlier, the forecast of the onset and the demise dates of the PFWS is plausible, given their close ties to the seasonal cycle. This is partially demonstrated by the CCSM4 hindcasts showing relatively smaller errors in the forecast of climatological onset date and demise dates at short lead times (Figure 2). The fact that the errors of the CCSM4 hindcasts in forecasting the climatological onset and demise dates grow with lead time suggests that the model drift is large.

The anomaly correlation is used as one of the metrics of assessing the fidelity of CCSM4 hindcasts in forecasting the onset and the demise dates of the PFWS (Figure 4a). Here, the anomaly correlation refers to the Pearson product–moment correlation coefficient between the observed and hindcasted ensemble-mean onset dates or demise dates. In a sobering display, CCSM4 hindcasts show that the anomaly correlations are very low at all lead times for both the onset dates and the demise dates, and there is no relationship to the hindcast lead time (Figure 4a).

Given the 10 ensemble members of the CCSM4 hindcasts, the signal-to-noise ratio to measure the ensemble spread of the hindcast can be computed. The signal-to-noise ratio is calculated as the variance of the signal (σ^2_{signal}) divided by the variance of the noise (σ^2_{noise}), which are given by:

$$\sigma^2_{\text{noise}} = \frac{1}{N(n-1)} \sum_{i=1}^{N} \sum_{j=1}^{n} \left(x_{ij} - \overline{x}_i\right)^2, \tag{3}$$

$$\sigma^2_{\text{signal}} = \sigma^2_{\text{EM}} - \frac{1}{n}\sigma^2_{\text{noise}}, \tag{4}$$

where,

$$\sigma^2_{\text{EM}} = \frac{1}{(N-1)} \sum_{i=1}^{N} \left(\overline{x}_i - \overline{\overline{x}}\right)^2, \tag{5}$$

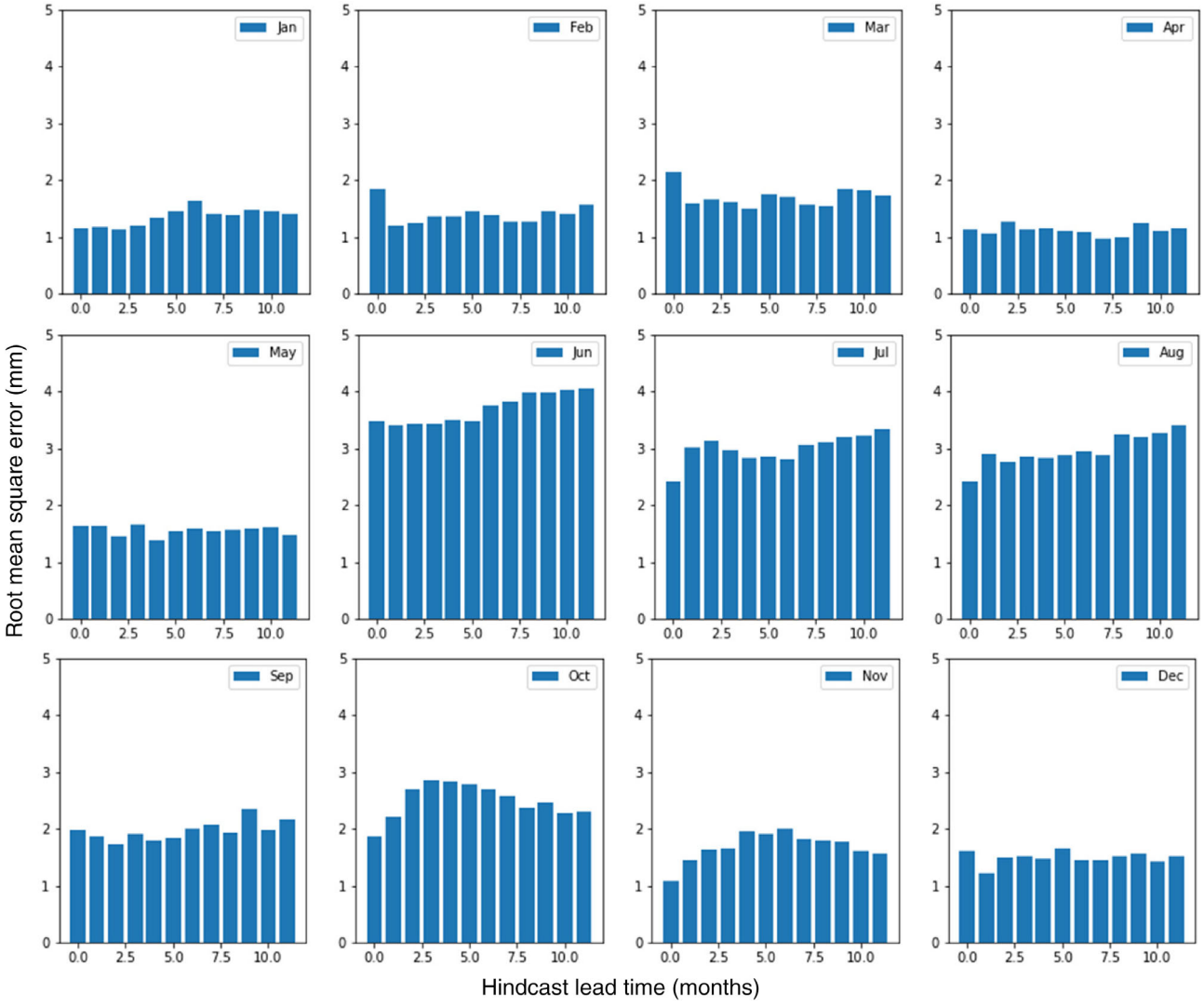

FIGURE 3 Root mean square error of monthly mean precipitation from CCSM4 hindcasts at lead times of 0–11 months

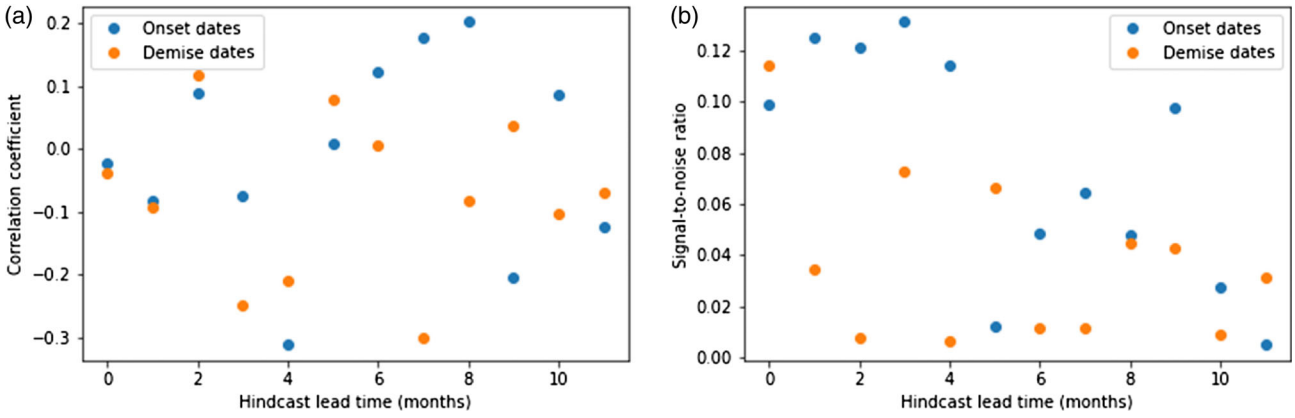

FIGURE 4 (a) The anomaly correlation between the 1983–2015 observed and CCSM4 hindcast onset dates (blue dots) and the anomaly correlation between the 1983–2015 observed and CCSM4 hindcast demise dates (orange dots) of the PF wet season at hindcast lead times of 0–11 months. (b) The same as (a), but for signal-to-noise ratio

where x_{ij} is a climate variable (e.g., onset date, demise date and seasonal rainfall), $i = 1,..., N$ is the number of years, $j = 1,...., n$ is the number of ensemble members, $\bar{x}_i$ is the ensemble mean for year i, and $\bar{\bar{x}}$ is the ensemble mean climatology of the variable.

The signal-to-noise ratio is computed for the onset and the demise dates of the PFWS at all hindcast lead times of 0–11 months (Figure 4b). The signal-to-noise ratios for the onset and the demise dates of the PFWS are very low at all hindcast lead times (Figure 4b), indicating high ensemble spread (or hindcast uncertainty) in predicting the onset and the demise dates of the PFWS. In a way, the result in Figure 4b is encouraging, considering that the anomaly correlation of the hindcast for the onset and demise dates of the PFWS is extremely low (Figure 4a). Another highlight of Figure 4b is that the signal-to-noise ratio does not show any increasing trend with lead time, which suggests that the model drift is not severe enough to make the ensemble members converge. Similarly, the signal-to-noise ratio of the monthly mean precipitation at all lead times (0–11 months) was computed. This calculation revealed that the ratio was the lowest in months comprising the PFWS (i.e., June–October) and highest in the boreal winter months (not shown). Interestingly, the signal-to-noise ratio of the CCSM4 hindcasts for the monthly mean precipitation throughout the year tends to decrease with lead time, suggesting the domination of internal variability as the hindcast evolves from initial time. In other words, one of the underlying reasons for the poor predictability of CCSM4 displayed in Figure 4 is that the PFWS is inherently chaotic.

3.2.2 | Probabilistic skill

Deterministic skill assessment is a quantitative assessment of the hindcast based on the ensemble mean. However, given the presence of chaotic variations of the climate system, an assessment of the forecast uncertainty is necessary. Several studies have argued that probabilistic forecasts, which, in fact, complement deterministic verification by quantifying uncertainty, are more informative and could bring greater value to the end users of the climate forecasts (Richardson, 2000, 2006; Palmer, 2002). In this study, we employ the area under the relative operating characteristic (ROC) curve (AUC) following Graham *et al*. (2000) and Misra (2004) to assess the probabilistic skill of CCSM4 hindcasts for anomalous onset and demise of the rainy season over PF. The details of computing AUC are provided in the Supplementary Section. In addition, we also compare the AUC of CCSM4 hindcasts for seasonal rainfall of the PFWS for fixed calendar months of the season and variable length of the season.

To assess the probabilistic skill of CCSM4 hindcasts in predicting the onset and the demise dates of the PFWS, ROC curves are created for hindcast lead times

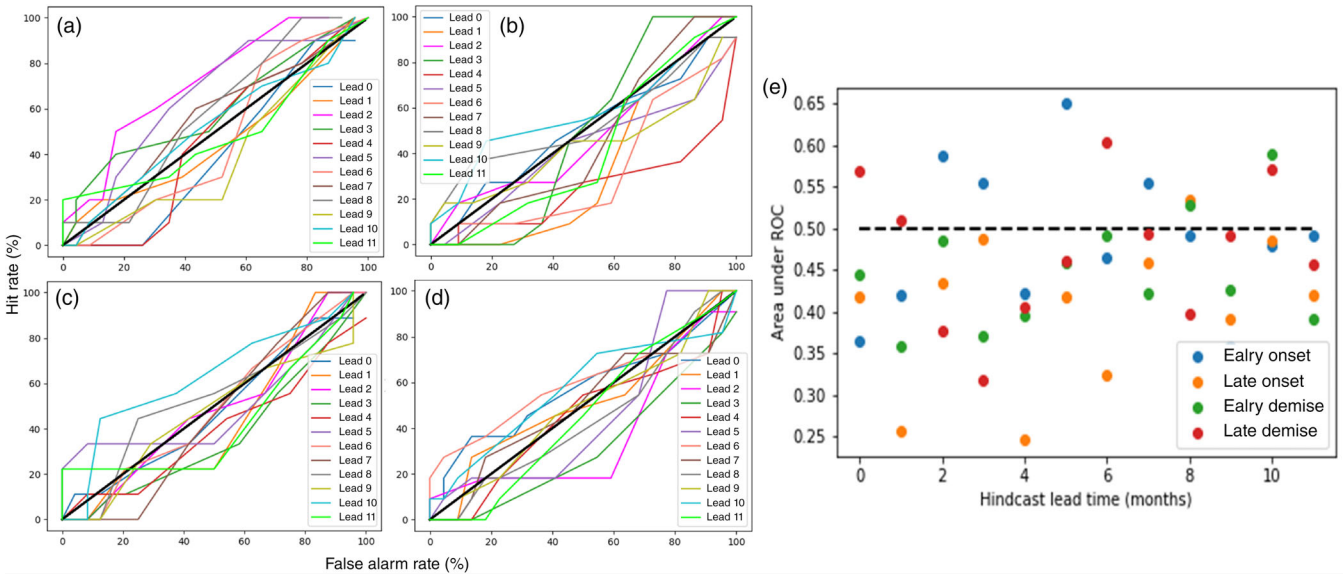

FIGURE 5 ROC curves for (a) early onset events, (b) late onset events, (c) early demise events and (d) late demise events from the CCSM4 hindcasts at lead times of 0–11 months. (e) The area under the ROC for early and late onset years, early and late demise years from CCSM4 hindcasts at lead times of 0–11 months

of 0–11 months for early onset events, late onset events, early demise events and late demise events (Figure 5a–d). The thresholds for these events are identified by ranking and separating the observed and the hindcast events into terciles. The ROC curves that bow to the upper left of the plot (or when AUC ≥0.5) represent a skilful hindcast. These ROC skill scores reveal that CCSM4's predictions of early onset and late demise of the PFWS may be slightly skilful at some lead times. However, CCSM4 is not skilful at predicting a late onset or an early demise of the PFWS (Figure 5). This is more apparent from the AUC displayed in Figure 5e.

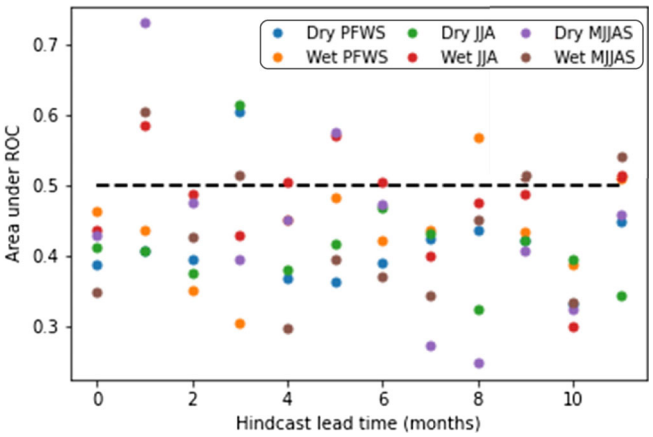

FIGURE 6 The area under the ROC curve, for dry (blue dot) and wet (orange dot) seasonal rainfall anomalies with variable seasonal length, fixed length JJA dry (green dot) and wet (red dot) seasonal rainfall anomalies and for extended fixed length MJJAS dry (purple dot) and wet (brown dot) seasonal rainfall anomalies from CCSM4 hindcasts at lead times of 0–11 months

To assess the probabilistic skill of CCSM4 hindcasts in predicting the seasonal rainfall of the PFWS, AUCs are computed for hindcasts at lead times of 0–11 months for dry and wet seasonal rainfall anomalies (Figure 6). The season is defined in three ways: June–July–August (JJA), extended fixed length season of May–June–July–August–September (MJJAS) and the varying seasonal length of the PFWS as it starts on the onset date and ends on the demise date of the year. The AUC in Figure 6 shows that CCSM4's predictions of summer seasonal rainfall anomalies, broadly construed, are generally unskilful, regardless of hindcast lead time.

3.3 | The North Atlantic subtropical high

CCSM4 exhibits a late bias in predicting both the onset date and the demise date of the PFWS. For the onset dates, the late bias increases with the increasing hindcast lead time (Figure 2). The aim of the analysis in this subsection is to understand why this late bias exists in the model hindcasts. The onset date and the demise date of the PFWS each coincide with changes in the prevailing 850 hPa wind direction over PF, associated with the seasonal migration of NASH (Misra *et al.*, 2018). The goal here is to understand the depiction of the NASH in the CCSM4 hindcasts.

The verification of the NASH strength and position in the CCSM4 seasonal hindcasts is conducted using sea level pressure data from the NCEP-DOE Reanalysis-2 (R2; Kanamitsu *et al.*, 2002). We note that the CCSM4 sea level pressure dataset is available from 1983 to 2014, whereas the CCSM4 precipitation dataset is available from 1983 to 2015, as indicated earlier. Figure 7a shows that the maximum central pressure of the NASH on the

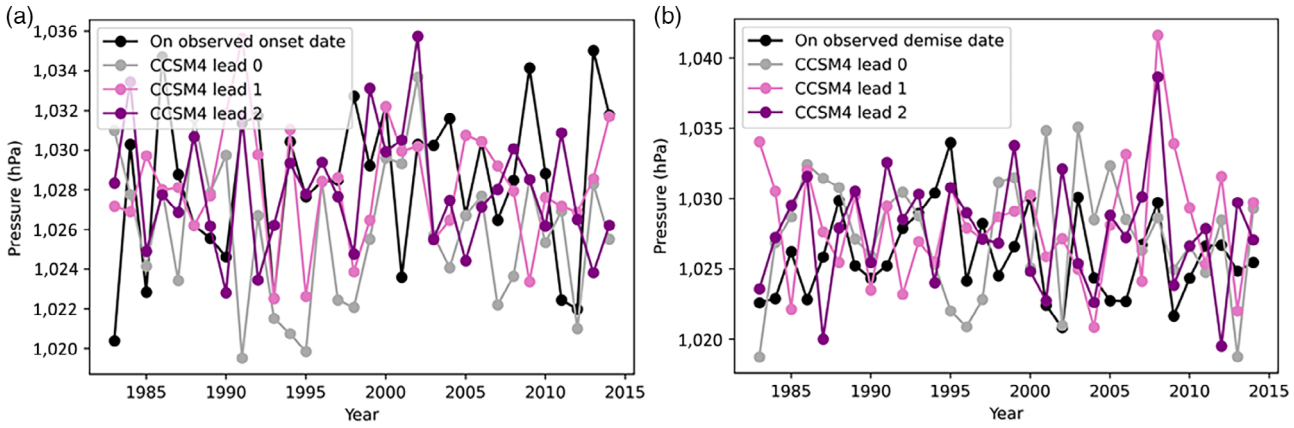

FIGURE 7 (a) The observed maximum sea level pressure in the domain 280°–350°E and 15°–45°N, valid on the observed onset date (black line), and model CCSM4 onset date hindcasted at lead times of 0, 1 and 2 months (grey, pink and purple lines, respectively). (b) The same as in (a), but valid on the demise dates

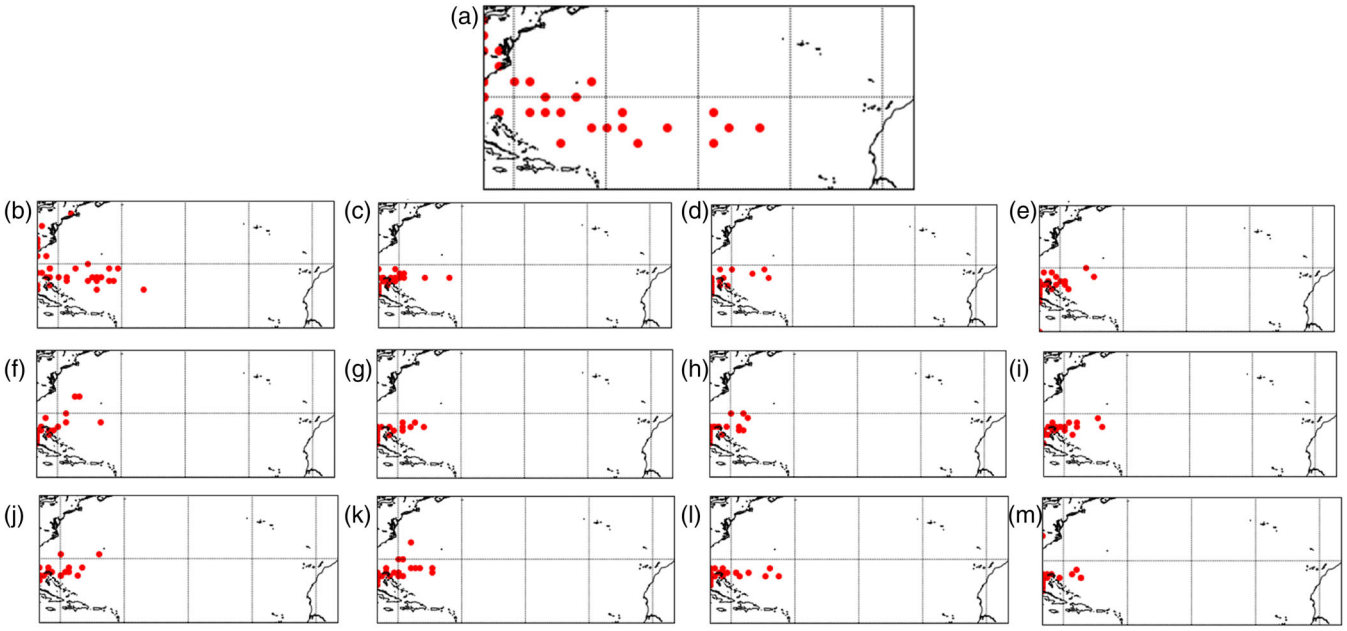

FIGURE 8 (a) The observed westernmost point on the 1,020 hPa isobar of the mean sea level pressure from R2 reanalysis on the observed onset dates of the PF wet season in 1983–2014. (b–m) The westernmost point on the 1,020 hPa isobar of the mean sea level pressure from CCSM4 hindcast at lead times of 0–11 months on the CCSM4 hindcast onset dates of the PF wet season in 1983–2014

observed onset dates in 1983–2014 falls between 1,020 and 1,035 hPa. The observed central sea level pressure valid on the onset dates hindcasted by the model at lead times of 0, 1 and 2 months also generally falls within the range of 1,020–1,035 hPa (Figure 7a). Likewise, the range of maximum sea level pressure values on the demise dates is also approximately 1,020–1,035 hPa (Figure 7b). We note that within the same year, there is little coherence among the central pressure values of the NASH on the observed and the hindcasted onset dates (Figure 7a). This may be attributed to the fact that the observed and model hindcasted onset dates are quite different from each other. The central pressure of the NASH on the demise dates also displays similar incoherence between the observed and hindcasted values (Figure 7b).

The westward extent of the NASH is analysed by noting the location of the westernmost point of the 1,020 hPa isobar. This contour is well defined, since the observed central sea level pressure of the NASH exceeds 1,020 hPa on the onset date of the PFWS in each of the years of the study period (1983–2014; Figure 7a). Furthermore, the 1,020 hPa contour defines the western boundary of the NASH affecting PF. Isobars lower than 1,020 hPa would be far into the continent and not necessarily represent the variations of NASH affecting PF. A similar argument was suggested in Li *et al.* (2011) who used 1,560 gpm to represent the western boundary migration of the NASH. The observed westernmost points of the 1,020 hPa isobar on the observed onset dates of the 1983–2014 PFWSs are scattered in the southern and the western regions of the North Atlantic, indicating that the westward extent or migration of the NASH is highly variable interannually on the onset date of the PFWS (Figure 8a). At hindcast lead times of 0–11 months, CCSM4 shows that the westernmost point of the 1,020 hPa isobar is in the southwest region of the North Atlantic on the model-hindcasted onset dates in most years from 1983 to 2014 (Figure 8b–m). The CCSM4 hindcasts erroneously predict a lower interannual variability of the westward extent of the NASH, and the error increases with hindcast lead time. Therefore, the systematic errors in the onset and demise of the PFWS in the CCSM4 hindcasts may be partially attributed to the rather sluggish variations of the westward extent of the NASH and incoherent variations of its strength with the observations.

4 | CONCLUSIONS

The results of this study indicate that the CCSM4 seasonal hindcasts have generally low predictive skill of the PFWS. CCSM4 hindcasts display a late bias in predicting the onset and the demise dates of the PFWS. In the case of the onset dates of the PFWS, the late bias of the CCSM4 hindcasts increases with lead time. The RMSE is

high for the demise dates of the PFWS in the CCSM4 hindcasts and even higher for the onset dates of the PFWS. For the onset dates only, the RMSE increases with hindcast lead time. The late bias and RMSE of the demise dates of the PFWS remain constant at hindcast lead times greater than 1 month. Perhaps, the most discouraging finding is the extremely low anomaly correlations between the observed and CCSM4 hindcasted onset and demise dates of the PFWS. However, given the poor anomaly correlations and RMSE values, a slightly comforting finding is that the CCSM4 seasonal hindcasts display low signal-to-noise ratios for the forecast of the onset and demise dates of the PFWS. This potentially suggests that the evolution of the PFWS is inherently chaotic.

The analyses of the RMSE and signal-to-noise ratio of the monthly mean precipitation highlight the low predictability of summer precipitation compared to the relatively high predictability of winter precipitation in PF. This finding is consistent with previous studies, which have noted the higher predictability of the winter season precipitation due to its teleconnection with ENSO (e.g., Stefanova *et al*., 2012).

The assessment of probabilistic skill shows that CCSM4 hindcasts may have some skill in predicting early onsets and late demises of the PFWS, but not late onsets or early demises of the PFWS. In addition, the probabilistic skill assessment reveals that CCSM4 seasonal hindcasts are broadly unskilful in predicting the seasonal rainfall anomalies for either fixed length or varying length PFWS.

Our study finds that some of this bias could be related to the poor rendition of the variability of the NASH in the CCSM4 hindcasts. The seasonal hindcasts display very poor coherence in the variations of the strength of the NASH both at onset and demise dates with the corresponding observations. In addition, the CCSM4 seasonal hindcasts do not capture the interannual variability in the westward extent of the NASH. The hindcasts are remarkably consistent in their depiction of the westward extent of the NASH, with the westernmost point of the 1,020 hPa isobar located in the southwest region of the North Atlantic on nearly all its hindcasted onset dates from 1983 to 2014. Furthermore, CCSM4 increasingly underestimates the interannual variability in the westward extent of the NASH with increasing lead time of the forecasts. Interannual variability in the position of the western ridge of the NASH contributes to interannual variability in summer precipitation in the southeast United States, potentially including the PFWS (Li *et al*., 2011). Therefore, the underestimation of the interannual variability of the position of the western ridge of the NASH is an issue to be addressed in the hindcast to improve the predictability of the PFWS.

ACKNOWLEDGEMENT

The support of NASA grant NNX17AG72G is acknowledged.

AUTHOR CONTRIBUTIONS

Carly Narotsky: Formal analysis; methodology; visualization; writing – original draft; writing – review and editing. **Vasubandhu Misra:** Conceptualization; funding acquisition; methodology; project administration; resources; supervision; writing – original draft; writing – review and editing.

ORCID

Carly D. Narotsky https://orcid.org/0000-0002-0182-2925

Vasubandhu Misra https://orcid.org/0000-0002-1345-6280

REFERENCES

Bombardi, R.J., Kinter, J.L. and Frauenfeld, O.W. (2019) A global gridded dataset of the characteristics of the rainy and dry seasons. *Bulletin of the American Meteorological Society*, 100, 1315–1328. https://doi.org/10.1175/BAMS-D-18-0177.1.

Camberlin, P. and Diop, M. (2003) Application of daily rainfall principal component analysis to the assessment of the rainy season characteristics in Senegal. *Climate Research*, 23, 159–169.

Chen, M., Shi, W., Xie, P., Silva, V.B.S. and Janowiak, J.E. (2008) Assessing objective techniques for gauge-based analyses of global daily precipitation. *Journal of Geophysical Research.*, 113, D04110.

Gent, P.R., Danabasoglu, G., Donner, L.J., Holland, M.M. and Zhang, M. (2011) The community climate system model version 4. *Journal of Climate*, 24, 4973–4991. https://doi.org/10.1175/2011JCLI4083.1.

Graham, R.J., Evans, A.D.L., Mylne, K.R., Harrison, M.S.J. and Robertson, K.B. (2000) An assessment of seasonal predictability using atmospheric general circulation models. *Quarterly Journal of the Royal Meteorological Society*, 126, 2211–2240.

Kanamitsu, M., Ebisuzaki, W., Woollen, J., Yang, S.-K. and Potter, G.L. (2002) NCEP–DOE AMIP-II reanalysis (R-2). *Bulletin of the American Meteorological Society*, 83, 1631–1643. https://doi.org/10.1175/BAMS-83-11-1631.

Kirtman, B.P., Min, D., Infanti, J.M., Kinter, J.L., III and Wood, E. F. (2014) The North American multimodel ensemble: Phase-1 seasonal-to-interannual prediction; Phase-2 toward developing intraseasonal prediction. *Bulletin of the American Meteorological Society*, 95, 585–601.

Kirtman, B.P., Misra, V., Burgman, R.J., Infanti, J.M. and Obeysekera, J. (2017) Florida climate variability and prediction. In: *Florida's Climate: Change, Variations, and Impacts*. Gainesville, FL: Florida Climate Insitute, pp. 511–532. Retrieved from: . https://doi.org/10.17125/fci2017.ch17.

Li, W., Li, L., Fu, R., Deng, Y. and Wang, H. (2011) Changes to the North Atlantic subtropical high and its role in the intensification of summer rainfall variability in the southeastern United States. *Journal of Climate*, 24, 1499–1506. https://doi.org/10.1175/2010JCLI3829.1.

Liebmann, B., Carmargo, S.J., Seth, A., Marengo, J.A. and Vera, C. S. (2007) Onset and end of the rainy season in South America in observations and the ECHAM 4.5 atmospheric general circulation model. *Journal of Climate*, 20, 2037–2050.

Lindsey, B.D., Berndt, M.P., Katz, B.G., Ardis, A.F. and Skach, K.A. (2009) Factors affecting water quality in selected carbonate aquifers in the United States, 1993–2005: U.S. Geological Survey Scientific Investigations Report 20085240, p. 117. https://pubs.er.usgs.gov/publication/sir20085240.

Misra, V. (2004) An evaluation of the predictability of austral summer season precipitation over South America. *Journal of Climate*, 17, 1161–1175.

Misra, V., Bhardwaj, A. and Mishra, A. (2018) Characterizing the rainy season of peninsular Florida. *Climate Dynamics*, 51, 2157–2167. https://doi.org/10.1007/s00382-017-4005-2.

Misra, V. and DiNapoli, S.M. (2013) Understanding the wet season variations over Florida. *Climate Dynamics*, 40, 1361–1372. https://doi.org/10.1007/s00382-012-1382-4.

Misra, V. and Mishra, A. (2016) The oceanic influence on the rainy season of Peninsular Florida. *Journal of Geophysical Research*, 121, 7691–7709. https://doi.org/10.1002/2016JD024824.

Misra, V., Mishra, A. and Bhardwaj, A. (2019) A coupled ocean-atmosphere downscaled climate projection for the Peninsular Florida region. *Journal of Marine Systems*, 194, 25–40.

National Wildlife Federation (NWF). (2019) The Everglades. [Accessed 18th July 2019] https://www.nwf.org/Educational-Resources/Wildlife-Guide/Wild-Places/Everglades.

Palmer, T.N. (2002) The economic value of ensemble forecasts as a tool for risk assessment. From days to decades. *Quarterly Journal of the Royal Meteorological Society*, 128, 747–774. https://doi.org/10.1256/0035900021643593.

Putnam, A.H. (2016) Florida Agriculture: By the Numbers., Florida Department of Agriculture and Consumer Services, Tallahassee, FL. https://www.nass.usda.gov/Statistics_by_State/Florida/Publications/Annual_Statistical_Bulletin/FL_Agriculture_Book/2016/Florida_Agriculture_by_the_Numbers_Brochure_2016.pdf.

Richardson, D.S. (2000) Skill and relative economic value of the ECMWF ensemble prediction system. *Quarterly Journal of the Royal Meteorological Society*, 126, 649–667. https://doi.org/10.1002/qj.49712656313.

Richardson, D.S. (2006) Predictability and economic value. In: Palmer, T. and Hagedorn, R. (Eds.) *Predictability of Weather and Climate*. Cambridge: Cambridge University Press, pp. 628–644. https://doi.org/10.1017/CBO9780511617652.

Slocum, M.G., Platt, W.J., Beckage, B., Panko, B. and Lushine, J.B. (2007) Decoupling natural and anthropogenic fire regimes: a case study in Everglades National Park, Florida. *Natural Areas Journal*, 27, 41–55.

Stefanova, L., Misra, V., O'Brien, J.J., Chassignet, E.P. and Hameed, S. (2012) Hindcast skill and predictability for precipitation and two-meter air temperature anomalies in global circulation models over the Southeast United States. *Climate Dynamics.*, 38, 161–173. https://doi.org/10.1007/s00382-010-0988-7.

Wang, B. (1995) Interdecadal changes in El Niño onset in the last four decades. *Journal of Climate*, 8, 267–285.

Wang, B. and An, S.-I. (2002) A mechanism for decadal changes of ENSO behavior: roles of background wind changes. *Climate Dynamics*, 18, 475–486.

Wang, C. and Picaut, J. (2004) Understanding ENSO physics - a review. In: Wang, C., Xie, S.-P. and Carton, J.A. (Eds.) *Earth's Climate: The Ocean-Atmosphere Interaction*. Geophysical Monograph Series, Vol. 147. Washington, DC: AGU, pp. 21–48.

Xie, P., Yatagai, A., Chen, M., Hayasaka, T. and Yang, S. (2007) A gauge-based analysis of daily precipitation over East Asia. *Journal of Hydrometeorology*, 8, 607–626.

Zhu, Z. and Li, T. (2016) A new paradigm for continental U.S. summer rainfall variability: Asia–North America teleconnection. *Journal of Climate*, 29, 7313–7327. https://doi.org/10.1175/JCLI-D-16-0137.1.

Zhu, Z. and Li, T. (2018) Amplified contiguous United States summer rainfall variability induced by East Asian monsoon interdecadal change. *Climate Dynamics*, 50, 3523–3536. https://doi.org/10.1007/s00382-017-3821-8.

SUPPORTING INFORMATION

Additional supporting information may be found in the online version of the article at the publisher's website.

How to cite this article: Narotsky, C. D., & Misra, V. (2021). The seasonal predictability of the wet season over Peninsular Florida. *International Journal of Climatology*, 1–10. https://doi.org/10.1002/joc.7423

Supplementary Material

The Seasonal Predictability of the Wet Season over Peninsular Florida

Carly D. Narotsky[1, 2, #] and Vasubandhu Misra[1, 2, 3]

[1]Department of Earth, Ocean, and Atmospheric Science, Florida State University, Tallahassee, Florida, U. S. A.

[2]Center for Ocean-Atmospheric Prediction Studies, Florida State University, Tallahassee, Florida, U. S. A.

[3]Florida Climate Institute, Florida State University, Tallahassee, Florida, U. S. A.

Corresponding author email: cnarotsky@fsu.edu

Procedure to compute area under the relative operating characteristic curve

1. Rank from 1 to 33 the observed onset dates from years 1983–2015. Separate the ranks into terciles to identify the observed threshold for early onset and the observed threshold for late onset.
2. Rank from 1 to 330 the onset dates hindcasted by the model at a lead of 0 months from all 33 years and 10 ensemble members. Separate into terciles and identify the model thresholds for early onset and late onset.
3. Examine the observed 1983 onset date. Is it an early onset (occurs in the first tercile, i.e., lower than the first threshold)?
    - If so, the answer is "yes" in the contingency table (Table S1). Go to (a).
    - If not, the answer is "no" in the contingency table (Table S1). Go to (b).

    a) Using the model threshold for early onset, ask:

    Do 10% (or 1 out of 10) ensemble members predict early onset in 1983? If yes, assign H=1. If no, assign M=1.

    Do 20% (or 2 out of 10) ensemble members predict early onset in 1983? If yes, assign H=1. If no, assign M=1.

    Continue like this up to 90% of ensemble members.

    b) Using the model threshold for early onset, ask:

    Do 10% (or 1 out of 10) ensemble members predict early onset in 1983? If yes, assign FA=1. If no, assign CR=1.

    Do 20% (or 2 out of 10) ensemble members predict early onset in 1983? If yes, assign FA=1. If no, assign CR=1.

    Continue like this up to 90% of ensemble members.

Repeat step 3 through all years.

4. For each percentage, sum up the values of H, M, FA, and CR across all years.
5. For each percentage, compute the Hit Rate (HR) and the False Alarm Rate (FAR).

$$HR=H/(H+M)$$

$$FAR=FA/(FA+CR).$$

6. Plot the Hit Rate against the False Alarm Rate. This is the Relative Operating Characteristic Curve (ROC). Compute the area under the ROC.
7. Repeat steps 3–6 for the event type "late onset".

Repeat steps 2–7 using the onset dates hindcasted by the model at each of the remaining lead times.

Repeat all steps for other event types such as "early demise", "late demise", "wet seasonal rainfall anomaly", and "dry seasonal rainfall anomaly".

	Ensemble probability for event exceeds threshold.	Ensemble probability for event does not exceed threshold.
Event is observed. "Yes"	Hit (H)	Miss (M)
Event is not observed. "No"	False Alarm (FA)	Correct Rejection (CR)

Table S1: Contingency table used for creating relative operating characteristic curves to quantify hindcast uncertainty.